With SI

MATER. RES. LETT., 2017
http://dx.doi.org/10.1080/21663831.2017.1280707

MATERIALS RESEARCH LETTERS
Taylor & Francis
Taylor & Francis Group

OPEN ACCESS

Rendering $Ti_3C_2T_x$ (MXene) monolayers visible

A. Miranda[a], J. Halim[b], A. Lorke[a] and M. W. Barsoum[b]

[a]Department of Physics and CENIDE, Universität Duisburg-Essen, Duisburg, Germany; [b]Department of Materials Science and Engineering, Drexel University, Philadelphia, PA, USA

ABSTRACT

Herein we report on how to render $Ti_3C_2T_x$ (MXene) monolayers deposited on SiO_2/Si wafers, with different SiO_2 thicknesses, visible. Inputting the effective thickness of a $Ti_3C_2T_x$ monolayer (1 ± 0.2 nm) measured by atomic force microscopy, and its refractive index into a Fresnel-law-based simulation software, we show that the optical contrast of $Ti_3C_2T_x$ monolayers deposited on SiO_2/Si wafers depends on the SiO_2 thickness, number of MXene layers, and the light's wavelength. The highest contrast was found for SiO_2 thicknesses around 220 nm. Simulations for other substrates, namely, Al_2O_3/Si, HfO_2/Si, Si_3N_4/Si and Al_2O_3/Al, are presented as supplementary information.

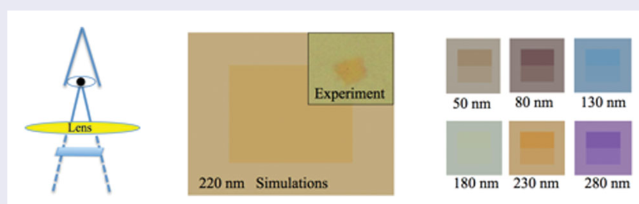

IMPACT STATEMENT

The experimental and simulated color contrasts between $Ti_3C_2T_x$ (MXene) monoflakes deposited on SiO_2 of various thicknesses—under an optical microscope—were obtained for the first time.

ARTICLE HISTORY
Received 7 October 2016

KEYWORDS
Optical microscope; optical properties; MXene monolayers; visibility

Introduction

Recent years have seen an increasing interest in the study of 2D materials and their practical applications [1–3] both alone or in stacked configurations [4,5]. This interest was catalyzed by a 2004 paper on graphene [6], and now extends toward other 2D materials such as boron nitride (BN) [7], transition metal dichalcogenides [8–10], and black phosphorous [11], among others.

MXenes—early transition metal carbides and/or nitrides, that are produced by the selective etching of the A layers from the MAX phases—represent the newest, and potentially largest, 2D family of solids [12–15]. The MAX phases, in turn, are a large (>70) family of layered ternary transition metal carbides, where M is an early transition metal, A is an A-group element (mostly groups 13 and 14), and X is C or/and N [16]. Because during etching, the A-group element layers such as Al and Ga are replaced by –O, –OH, and –F terminations [17,18], the proper designation of the resulting 2D material is $M_{n+1}C_nT_x$, where T represents a surface termination, which can be O, OH, and/or F [17].

The most studied MXene to date is $Ti_3C_2T_x$, which has already shown potential for use in a number of diverse applications, such as batteries [19,20], supercapacitors [21,22], fuel cells [23], sensors [24,25], transparent conducting electrodes [26,27], photocatalytic applications [28], and water treatment [29] among others [30–33]. Most, if not all, of the aforementioned work has been carried out on multilayers and/or films, both thick and thin.

Recently, we reported on electric transport in single, free-standing isolated $Ti_3C_2T_x$ monolayers where we showed that at $\approx 1 \times 10^{28}\ m^{-3}$, the density of mobile carriers in this material is quite high [34]. Even more recently, we reported on conductive transparent spin-coated $Ti_3C_2T_x$ films, with high figures of merit [27]. During the course of that work, both the real, n, and imaginary, k, optical constants of these spincast films

CONTACT M. W. Barsoum barsoumw@drexel.edu Department of Materials Science and Engineering, Drexel University, Philadelphia, PA19104, USA

Supplemental data for this article can be accessed here. http://dx.doi.org/10.1080/21663831.2017.1280707

© 2017 The Author(s). Published by Informa UK Limited, trading as Taylor & Francis Group.
This is an Open Access article distributed under the terms of the Creative Commons Attribution License (http://creativecommons.org/licenses/by/4.0/), which permits unrestricted use, distribution, and reproduction in any medium, provided the original work is properly cited.

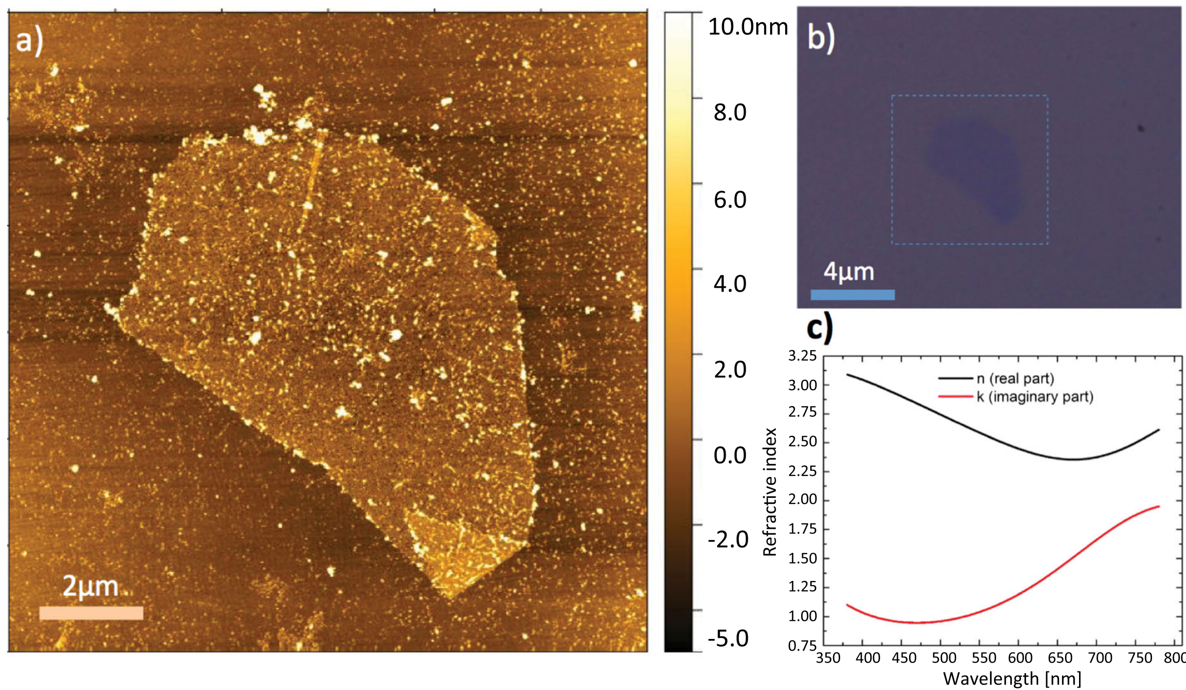

Figure 1. (a) AFM scan of a $Ti_3C_2T_x$ monolayer on a 285 nm thick SiO_2 substrate. Average height between flake and substrate is 1.8 ± 0.3 nm. AFM measurements of the folded corner are more reliable as they are less influenced by instrumental offsets and other artifacts. These measurements show a reproducible step of 1 ± 0.2 nm, which is the value assumed herein. Small bright regions in (a) are residues from the MXene dispersion; (b) visible spectrum unfiltered OM images of same flake—located in the center of the dotted frame—in which the folded MXene corner appears slightly darker. (c) Ellipsometric measurements of the real, *n*, and imaginary, *k*, parts of the refractive indices of $Ti_3C_2T_x$ as a function of wavelength in the visible region, reproduced from Ref. [27].

were measured [27]. Since as discussed below, *n* and *k* are important input parameters in our modeling, it is important to briefly explain how they were measured and why it is justifiable to use these values here. First, both single flakes and films were spincast from nominally identical colloidal solutions. Second, given that *n* and *k* are typically functions of film thickness, it would have been ideal if the values used herein were those measured on monolayered films. However, since currently such films do not exist, we chose instead to use the *n* and *k* values (Figure 1(c)), measured ellipsometrically on a 75 nm thick spincoated $Ti_3C_2T_x$ film. The details can be found in supplementary information of Ref. [27].

As far as we are aware, that information has yet to be exploited to render MXenes visible under an optical microscope (OM), in the same way that, for example, Blake et al. [35] and others [36–39], rendered single graphene layers visible. The same was done for single layers of transition metal dichalcogenides [40], BN [41], and other 2D systems [42]. The capability to quickly and accurately distinguish single from multiple flakes is a crucial requisite first step for using MXenes in microelectronic devices. To be able to do so rapidly and accurately with nothing more sophisticated than an OM is therefore important. The purpose of this work is to delineate the conditions under which $Ti_3C_2T_x$ monolayers, deposited on oxidized Si wafers, would be visible under an OM. To that effect, we measured the thicknesses of various flakes—deposited on substrates with varying SiO_2 thicknesses—using atomic force microscopy (AFM). We then combined these results, with the refractive indices of $Ti_3C_2T_x$ [27], to predict the best conditions to visualize $Ti_3C_2T_x$ monoflakes in an OM for a variety of substrates.

The $Ti_3C_2T_x$ flakes were produced by selective etching of Al from Ti_3AlC_2. The details can be found elsewhere [34]. To deposit single $Ti_3C_2T_x$ flakes, they were first dispersed in water—with a concentration of ≈ 1 to 2 mg/ml—and spincoated on Si wafers. For the latter, a drop was placed on the substrate and the spincoater was accelerated from 0 to 6000 rpm in 1 s and held at that speed for 60 s. The substrates were then inspected under an OM. Flakes, presumed to be monolayers, were scanned by tapping mode AFM. The difference in height between the monolayers and the Si substrate was measured to be 1.8 ± 0.3 nm, which overestimates the real thickness because of anomalies related to the measuring conditions of the AFM [43], instrument offset [44], and

other artifacts [45,46], as well as the possible presence of adsorbates on top of the flakes in addition to surface terminations. The same is true of graphene where control experiments on monolayered graphene flakes revealed them to be offset by about ≈ 0.6 nm under the same experimental and environmental conditions. To solve this problem, the 2D community has concluded that folded regions give the most reliable measurements of thickness (see, e.g. [47]). Measurements on folded flakes here provided a reproducible thickness of 1 ± 0.2 nm, for a $Ti_3C_2T_x$ monolayer, in agreement with the SiO_2-MXene step height (1.8 ± 0.3 nm) reduced by the determined offset of ≈ 0.6 nm. It is important to note that, based on X-ray diffraction measurements, half the c-axis lattice parameter of $Ti_3C_2T_x$ is ≈ 1 nm [12]. Therefore, all such flakes were deemed single-layered.

Figure 1(a) shows the AFM scan for a monolayer MXene flake deposited on a Si wafer with a nominally 300 nm thick SiO_2 layer. In the AFM scan shown in Figure 1(a), small particulates are imaged both on the MXene and substrate. These particulates are most probably small oxide particles that form during MXene production and need further investigation. The largest of these particles are detectable under an OM and have been avoided when selecting regions for colorimetric evaluations. An OM micrograph taken using the whole range of visible light is shown in Figure 1(b).

Figure 1(c) shows the functional dependencies of n and k of $Ti_3C_2T_x$, on wavelength, λ, in the visible range (380–780 nm), which is the region of interest for this work. These values are taken from Ref. [27] and are reproduced here because the colorimetric simulations are based on them. Interestingly, we note that the average values of n and k in this region (2.6 and 1.3) are comparable to those of graphene in the same spectral window [48,49].

Similar to what was done for other 2D systems [35,40], we model our MXene sample as a stacked structure (Figure 2(a)) composed of air (layer 0, with refractive index n_0), MXene (layer 1, with thickness d_1 and refractive index n_1), SiO_2 (layer 2, with thickness d_2 and refractive index n_2 [50,51], and Si (layer 3, with refractive index n_3 [52]. Under these conditions, the MXene reflectivity is given by [53]:

$$R_{\mathrm{MXene}} = \left| \frac{r_1\, e^{i(\phi_1+\phi_2)} + r_2\, e^{-i(\phi_1-\phi_2)} + r_3\, e^{-i(\phi_1+\phi_2)} + r_1 r_2 r_3\, e^{i(\phi_1-\phi_2)}}{e^{i(\phi_1+\phi_2)} + r_1 r_2\, e^{-i(\phi_1-\phi_2)} + r_1 r_3\, e^{-i(\phi_1+\phi_2)} + r_2 r_3\, e^{i(\phi_1-\phi_2)}} \right|^2, \quad (1)$$

where $r_1 = (n_0 - n_1)/(n_0 + n_1)$, $r_2 = (n_1 - n_2)/(n_1 + n_2)$, and $r_3 = (n_2 - n_3)/(n_2 + n_3)$ are the relative changes in the index of refraction and $\phi_i = 2\pi n_i d_i/\lambda$ are the phase shifts in the various regions of the optical path for a given λ. Similarly, the substrate without MXene has a reflectivity expressed by $R_{\mathrm{Sub}} = |(r_2'\, e^{i\phi_2} + r_3\, e^{-i\phi_2})/(e^{i\phi_2} + r_2' r_3\, e^{-i\phi_2})|^2$, where $r_2' = (n_0 - n_2)/(n_0 + n_2)$. The absolute contrast for a MXene monolayer for a given λ is defined as:

$$C = \left| \frac{R_{\mathrm{MXene}} - R_{\mathrm{Sub}}}{R_{\mathrm{MXene}}} \right|. \quad (2)$$

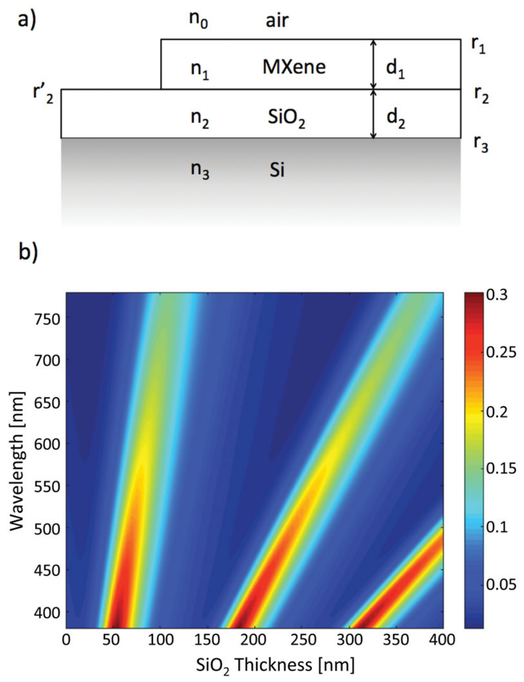

Figure 2. (a) Schematic of simulated MXene/SiO_2/Si trilayer modeled. (b) Color plot of the contrast as a function of SiO_2 thickness and λ for $Ti_3C_2T_x$ monolayers. Note the strong dependence on both λ and SiO_2 thickness. Three regions with high contrast can be easily seen. These regions delineate the best experimental conditions for the visualization of a $Ti_3C_2T_x$ monolayer. The color scale on the right shows the expected contrast.

When this equation is plotted for a single $Ti_3C_2T_x$ layer as a function of SiO_2 thickness and λ (Figure 2(b)), three regions of high contrast are found. These represent the optimal experimental conditions for the identification of single $Ti_3C_2T_x$ layers on SiO_2. They roughly follow the relation $2 \cdot d_{SiO_2} \cdot n_{SiO_2} = (m + 1/2)\lambda$, with $m = 0, 1, 2$, corresponding to the optical path being a half-integer times the wavelength. This formula indicates that these Fabry-Perot-type resonances come from standing waves in the SiO_2 and reflection at an open end (antinode) on the MXene-SiO_2 interface side and reflection at a fixed end (node) on the Si–SiO_2 interface side. Figure 3(a–c) show the contrast between 1 (bottom curve) to 5 (top curve) layers of $Ti_3C_2T_x$ as a function of SiO_2 thickness for monochromatic blue, green, and red light, respectively. Note that the position of the absolute contrast maxima for each λ is independent of the number of MXene layers.

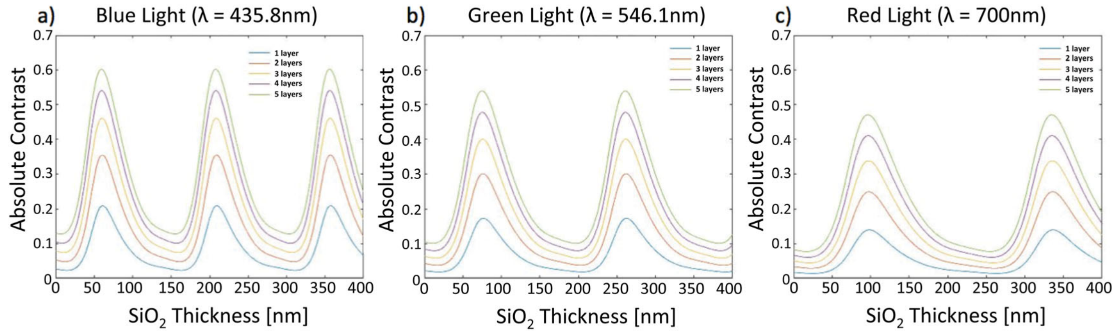

Figure 3. Color plot of the absolute contrast as a function of SiO_2 thickness for 1–5 $Ti_3C_2T_x$ layers predicted for, (a) blue (435.8 nm), (b) green (546.1 nm), and (c) red (700 nm) light. The contrast maxima vary for each λ, but are not functions of the number of MXene layers.

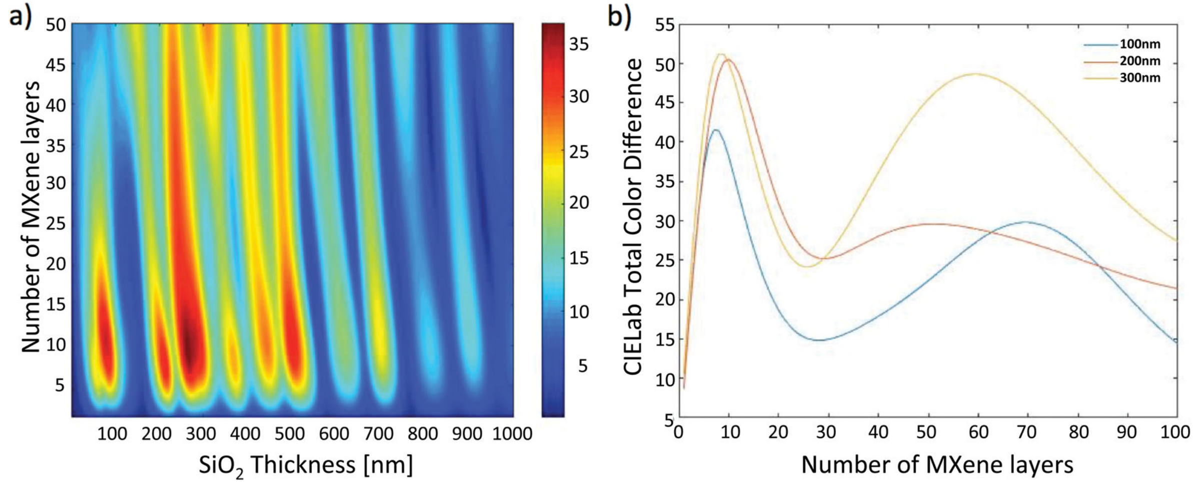

Figure 4. (a) Color plot of contrast between SiO_2 and $Ti_3C_2T_x$ monolayers as a function of the number of the latter and the thickness of the former observed under a tungsten lamp delineating the experimental conditions for which the contrast would be greatest; (b) Contrast difference as a function of 1–100 $Ti_3C_2T_x$ layers for three different SiO_2 thicknesses. Contrast depends on number of $Ti_3C_2T_x$ monolayers and peaks around 8–12 layers. For the thickest SiO_2 layer, a second maximum is seen around 60 layers. Herein each monolayer is assumed to be 1 nm.

Since these results pertain to a single λ, they are not of much use in an OM without filters, where all frequencies need to be taken into account. In that case, the colorimetric CIE 1931 XYZ [54] space should be calculated for visible wavelengths as:

$$\begin{pmatrix} X_j \\ Y_j \\ Z_j \end{pmatrix} = P \int_{380\,\text{nm}}^{780\,\text{nm}} S(\lambda)R(\lambda) \begin{pmatrix} \bar{x}(\lambda) \\ \bar{y}(\lambda) \\ \bar{z}(\lambda) \end{pmatrix} \mathrm{d}\lambda \tag{3}$$

where $\bar{x}(\lambda)$, $\bar{y}(\lambda)$, and $\bar{z}(\lambda)$ are the CIE 1931 matching functions, respectively (See Ref. [54] for selected colorimetric tables), $R(\lambda)$ is the reflectivity of the system, $S(\lambda)$ is the spectrum of the incident light source, that depends on the type of illumination and P is the total illumination power. The incident light source used here is an incandescent tungsten-filament light with a temperature of 2856 K, the most common source of light in OMs and thus illuminant A is used. It is described by a Planck's distribution law (shown in the supplementary information (SI)) and tabulated in Ref. [54]. Once the CIE 1931 XYZ color space is calculated, it is transformed to the CIELab color space which offers a more perceptual uniformity [39,54], by operating the transformations [39]:

$$L^* = 116 f\left(\frac{Y}{Y_n}\right) - 16, \quad a^* = 500\left[f\left(\frac{X}{X_n}\right) - f\left(\frac{Y}{Y_n}\right)\right],$$
$$b^* = 200\left[f\left(\frac{Y}{Y_n}\right) - f\left(\frac{Z}{Z_n}\right)\right], \tag{4}$$

where X_n, Y_n, and Z_n are the coordinates for the white point of the reference illuminant (109.850, 100, and 35.585, respectively, in case of illuminant A) and

$$f = \begin{cases} t^{1/3} & \text{if } t > (6/29)^3 \\ \frac{1}{3}(29/6)^2 t + \frac{4}{29} & \text{otherwise} \end{cases}. \tag{5}$$

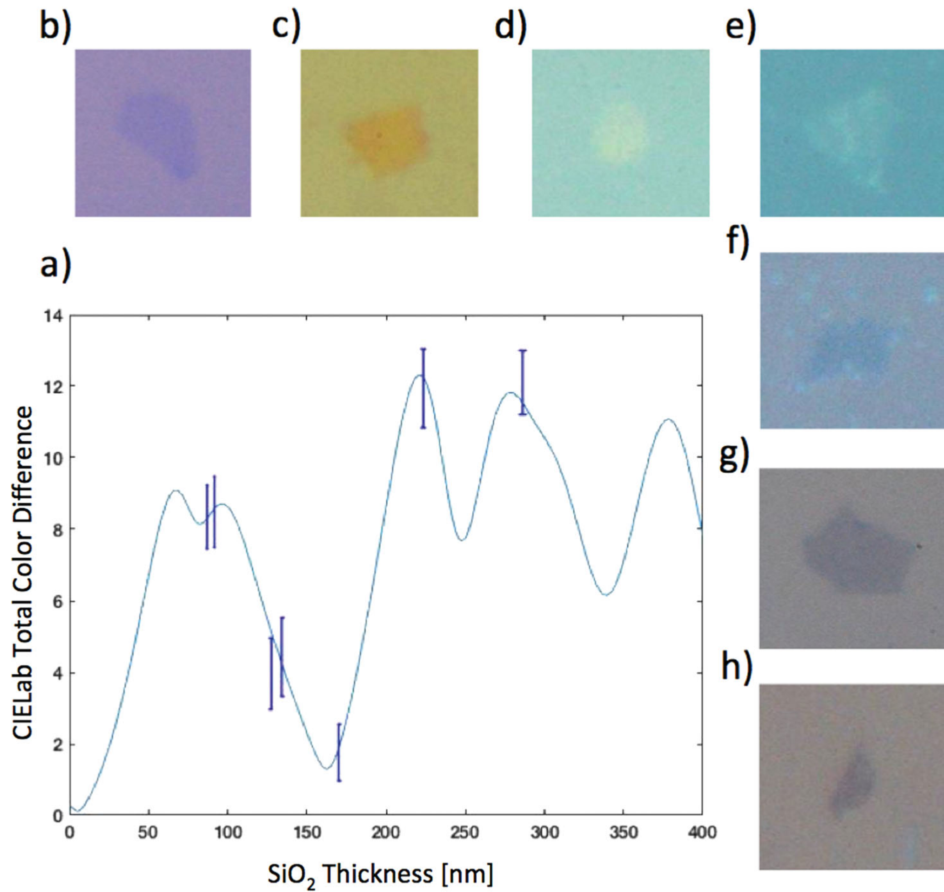

Figure 5. (a) Total color difference of a Ti3C2T*x* monolayer as a function of the SiO_2 layer thickness. Error bars represent experimental values for samples with the corresponding SiO_2 thicknesses. (b–h) OM images of $Ti_3C_2T_x$ monolayers on SiO_2 with thicknesses of 285, 223, 170, 134, 127, 90, and 87 nm, respectively, to which the data points in (a) correspond. All micrographs have dimension of $20 \times 20\ \mu m^2$. Flakes were illuminated by a standard W-lamp, without filters under the same experimental and environmental conditions (clean room controlled temperature and humidity). The luminosity of these pictures was adjusted in order to have a consistent color balance between experiment and simulations [38]. The experimentally measured CIELab total color differences are in quite good agreement with the calculations.

Lastly, we use the total color difference, TCD, defined as

$$TCD_{CIE76} = \sqrt{(\Delta L^*)^2 + (\Delta a^*)^2 + (\Delta b^*)^2}, \quad (6)$$

as the colorimetric distance between two colors.

Figure 4(a) shows the calculated color contrast between bare and $Ti_3C_2T_x$ covered substrates as a function of the number of monolayers—up to 50—and the thickness of the SiO_2, observed under a W-lamp (Illuminant A), delineating the experimental conditions for which the contrast would be largest. Here again there are combinations of the number of layers and SiO_2 thicknesses that result in bands of high contrast. When the same results are plotted as a function of the number of MXene layers—for three different SiO_2 thicknesses, 100, 200, and 300 nm (Figure 4(b))—the contrast curves have maxima between 8 and 12 layers before decreasing. Interestingly, there is second peak—at around 60 layers for the thickest SiO_2 substrates—possibly a Fabry-Perot resonance in the MXene layer.

Since herein we were particularly interested in identifying single flakes, Figure 5(a) plots the color contrast for the latter as a function of SiO_2 thickness. These results predict that a SiO_2 thickness of 222 nm provides the highest contrast. To test this prediction, we deposited single MXene layers on SiO_2/Si substrates of different thicknesses. The latter were prepared by etching standard Si wafers—with 285 nm thick, thermally grown SiO_2 (CrysTec, Berlin, Germany)—in buffered HF (20%) for 15, 30, 60, 90, and 120 s, which resulted in SiO_2 thicknesses of 223, 170, 134, 127, and 87 nm, respectively. To determine the SiO_2 thicknesses, a set of wafers—with a 285 nm thick thermal oxide—were etched, as above, with part of the wafer masked. A profilometer was then used to measure the step height between the etched and un-etched regions yielding the SiO_2 thickness. These measurements were confirmed by a colorimetric comparison between

the color of SiO_2 of the etched samples and the calculated ones for the measured thicknesses. To complete the set, a 90 nm thick SiO_2 layer thermally grown on Si (CrysTec Berlin, Germany) was also used.

When the TCD simulations (solid line in Figure 5(a)) and the experimental results (data points with error bars in Figure 5(a)) are compared, it is obvious that the agreement is quite good. The images were taken with a camera (Canon EOS 500D), attached to an OM (Zeiss Axiotech) with a 100 X objective and a numerical aperture of 0.75. The results (Figure 5(b–h)) are shown after luminosity balancing (full procedure for balancing and comparison between theory and experiments is discussed in the SI). The experimental results confirm that the best contrast is achieved with a SiO_2 thickness of 223 nm, where TCD peaks at ≈ 12 (Figure 5(c)) in excellent agreement with our theoretical predictions (12.3 at 222 nm). Interestingly, the second highest peak of visibility is calculated to be around 280 nm with a TCD of 11.8 (confirmed by a measured value of 11.5 at 285 nm). This thickness would allow good visibility for both MXene and graphene. It is worth noting that the thickness of every flake shown in Figure 5(b–h) was measured by AFM before observing them in the OM. Only single flakes were imaged in the OM and used.

In conclusion, making use of Fresnel's theory, we delineate the conditions under which MXene mono- and, in principle, multilayers can be rendered visible under an OM—using a W-lamp—after deposition on Si wafers with various SiO_2 thicknesses. Our simulations predict that SiO_2 thicknesses of 222 and 280 nm should result in the best contrast as observed experimentally. This work establishes a framework for detecting single MXene flakes on Si and other substrates. Colorimetric results on other substrates, such as Al_2O_3/Si, HfO_2/Si, Si_3N_4/Si and Al_2O_3/Al, with other illuminants (D65), present a shift of the maxima of contrast, but are similar in general to those on silica. For further details about these results and details of our methodology refer to the SI.

Funding

This work was funded by Ceramics Division of NSF (DMR-1310245) and Swedish Foundation for Strategic Research (Synergy Grant FUNCASE).

References

[1] Fiori G, Bonaccorso F, Iannaccone G, et al. Electronics based on two-dimensional materials. *Nat Nanotech*. 2014;9:768–779.

[2] Ferrari AC, Bonaccorso F, Fal'ko V, et al. Science and technology roadmap for graphene, related two-dimensional crystals, and hybrid systems. *Nanoscale*. 2015;7:4598–4810.

[3] Gupta A, Sakthivel T, Seal S. Recent development in 2D materials beyond graphene. *Prog Mater Sci*. 2015;73:44–126.

[4] Niu T, Li A. From two-dimensional materials to heterostructures. *Prog Surf Sci*. 2015;90:21–45.

[5] Geim AK, Grigorieva IV. Van der Waals heterostructures. *Nature*. 2013;499:419–425.

[6] Novoselov KS, Geim AK, Morozov SV, et al. Electric field effect in atomically thin carbon films. *Science*. 2004;306:666–669.

[7] Ci L, Song L, Jin C, et al. Atomic layers of hybridized boron nitride and graphene domains. *Nat Mater*. 2010;9:430–435.

[8] van der Zande AM, Huang PY, Chenet DA, et al. Grains and grain boundaries in highly crystalline monolayer molybdenum disulphide. *Nat Mater*. 2013;12:554–561.

[9] Duan X, Wang C, Pan A, et al. Two-dimensional transition metal dichalcogenides as atomically thin semiconductors: opportunities and challenges. *Chem Soc Rev*. 2015;44:8859–8876.

[10] Allain A, Kis A. Electron and hole mobilities in single-layer WSe_2. *ACS Nano*. 2014;8:7180–7185.

[11] Liu H, Du Y, Deng Y, et al. Semiconducting black phosphorus: synthesis, transport properties and electronic applications. *Chem Soc Rev*. 2015;44:2732–2743.

[12] Naguib M, Kurtoglu M, Presser V, et al. Two dimensional nanocrystals produced by exfoliation of Ti_3AlC_2. *Advan Mater*. 2011;23:4248–4253.

[13] Naguib M, Come J, Dyatkin B, et al. MXene: a promising transition metal carbide anode for lithium-ion batteries. *Electrochem Commun*. 2012;16:61–64.

[14] Mashtalir O, Naguib M, Dyatkin B, et al. Kinetics of aluminum extraction from Ti_3AlC_2 in hydrofluoric acid. *Mater Chem Phys*. 2013;139:147–152.

[15] Naguib M, Mochalin VN, Barsoum MW, et al. MXenes: a new family of two dimensional materials. *Advan Mater*. 2014;26:992–1005.

[16] Barsoum MW. *MAX: phases properties of machinable carbides and nitrides*. Weinheim: Wiley VCH GmbH & Co.; 2013.

[17] Halim J, Cook KM, Naguib M, et al. X-ray photoelectron spectroscopy of select multi-layered transition metal carbides (MXenes). *Appl Surf Sci*. 2016;362:406–417.

[18] Halim J, Kota S, Lukatskaya MR, et al. Synthesis and characterization of 2D molybdenum carbide (MXene). *Adv Funct Mater*. 2016;26:3118–3127.

[19] Liang X, Garsuch A, Nazar LF. Sulfur cathodes based on conductive MXene nanosheets for high performance lithium–sulfur batteries. *Angew Chem Inter Ed*. 2015;54:3907–3911.

[20] Er D, Li J, Naguib M, et al. Ti_3C_2 MXene as a high capacity electrode material for metal (Li, Na, K, Ca) Ion batteries. *ACS Appl Mater Interfaces*. 2014;6(14):11173–11179.

[21] Lukatskaya MR, Mashtalir O, Ren CE, et al. Cation intercalation and high volumetric capacitance of two-dimensional titanium carbide. *Science*. 2013;341:1502–1505.

[22] Ghidiu M, Lukatskaya, MR, Zhao MQ, et al. Conductive two-dimensional titanium carbide 'clay' with high volumetric capacitance. *Nature*. 2014;516:78–81.

[23] Xie X, Chen S, Ding W, et al. An extraordinarily stable catalyst: Pt NPs supported on two-dimensional $Ti_3C_2X_2$ (X = OH, F) nanosheets for oxygen reduction reaction. *Chem Comm*. 2013;49:10112–10114.

[24] Liu H, Duan C, Yang C, et al. A novel nitrite biosensor based on the direct electrochemistry of hemoglobin immobilized on MXene-Ti_3C_2. *Sensors Actuators B: Chem*. 2015;218:60–66.

[25] Chen J, Chen K, Tong D, et al. CO_2 and temperature dual responsive 'Smart' MXene phases. *Chem Comm*. 2015;51:314–317.

[26] Halim J, Lukatskaya, MR, Cook K, et al. Transparent conductive two-dimensional titanium Carbide epitaxial thin films. *Chem Mater*. 2014;26:2374–2381.

[27] Dillon AD, Ghidiu MJ, Krick AL, et al. Highly conductive optical quality solution-processed films of 2D titanium carbide. *Adv Funct Mater*. 2016;26:4162–4168.

[28] Mashtalir O, Cook KM, Mochalin VN, et al. Dye adsorption and decomposition on two-dimensional titanium carbide in aqueous media. *J Mater Chem A*. 2014;2:14334–14338.

[29] Peng Q, Guo J, Zhang Q, et al. Unique lead adsorption behavior of activated hydroxyl group in two-dimensional titanium carbide. *J Am Chem Soc*. 2014;136:4113–4116.

[30] Anasori B, Lukatskaya M, Gogotsi, Y. 2D metal carbides and nitrides (MXenes) for energy storage. *Nat Mater Rev*. doi:10.1038/natrevmats.2016.98

[31] Bhimanapati GR, Lin Z, Meunier V, et al. Recent Advances in two-dimensional materials beyond graphene. *ACS Nano*. 2015;9:11509–11539.

[32] Lei JC, Zhang X, Zhou Z. Recent advances in MXene: Preparation, properties, and applications. *Front Phys*. 2015;10:107303.

[33] Zhang H. Ultrathin Two-dimensional nanomaterials. *ACS Nano*. 2015;9:9451–9469.

[34] Miranda A, Halim J, Barsoum MW, et al. Electronic properties of freestanding $Ti_3C_2T_x$ MXene monolayers. *Appl Phys Lett*. 2016:108:033102.

[35] Blake P, Hill EW, Castro Neto AH, et al. Making graphene visible. *Appl Phys Lett*. 2007;91:063124.

[36] Jung I, Pelton M, Piner R, et al. Simple approach for high-contrast optical imaging and characterization of graphene-based sheets. *Nano Lett*. 2007;7:3569–3575.

[37] Roddaro S, Pingue P, Piazza V, et al. The optical visibility of graphene: interference colors of ultrathin graphite on SiO_2. *Nano Lett*. 2007;7:2707–2710.

[38] Ni ZH, Wang HM, Kasim J, et al. Graphene thickness determination using reflection and contrast spectroscopy. *Nano Lett*. 2007;7:2758–2763.

[39] Gao L, Ren W, Li F, et al. Total color difference for rapid and accurate identification of graphene. *ACS Nano*. 2008;2:1625–1633.

[40] Benameur MM, Radisavljevic B, Heron JS, et al. Visibility of dichalcogenide nanolayers. *Nanotech*. 2011;22:125706.

[41] Gorbachev RV, Riaz I, Nair RR, et al. Hunting for monolayer boron nitride: optical and Raman signatures. *Small*. 2011;7:465–468.

[42] Müller MR, Gumprich A, Ecik E, et al. Visibility of two-dimensional layered materials on various substrates. *J Appl Phys*. 2015;118:145305.

[43] Nemes-Incze P, Osváth Z, Kamarás K, et al. Anomalies in thickness measurements of graphene and few layer graphite crystals by tapping mode atomic force microscopy. *Carbon*. 2008;46:1435–1442.

[44] Mechler Á, Kopniczky J, Kokavecz J, et al. Anomalies in nanostructure size measurements by AFM. *Phys Rev B*. 2005;72:125407.

[45] Kühle A, Sorensen AH, Zandbergen JB, et al. Contrast artifacts in tapping tip atomic force microscopy. *Appl Phys A: Mater Sci Process*. 1998;66:S329–S332.

[46] Mechler Á, Kokavecz J, Heszler P, et al. Surface energy maps of nanostructures: atomic force microscopy and numerical simulation study. *Appl Phys Lett*. 2003;82:3740–3742.

[47] Novoselov KS, Jiang D, Schedin F, et al. Two-dimensional atomic crystals. *Proc Natl Acad Sci USA*. 2005;102:10451–10453.

[48] Cheon S, Kihm KD, Kim Hg, et al. How to reliably determine the complex refractive index (RI) of graphene by using two independent measurement constraints. *Scien Rep*. 2014;4:6364.

[49] Bruna M, Borini S. Optical constants of graphene layers in the visible range. *Appl Phys Lett*. 2009;94:031901.

[50] Herzinger CM, Johs B, McGahan WA, et al. Ellipsometric determination of optical constants for silicon and thermally grown silicon dioxide via a multi-sample, multi-wavelength, multi-angle investigation. *J Appl Phys*. 1998;83:3323–3336.

[51] Ghosh G. Dispersion-equation coefficients for the refractive index and birefringence of calcite and quartz crystals. *Opt Commun*. 1999;163:95–102.

[52] Jellison Jr G, Chisholm M, Gorbatkin S. Optical functions of chemical vapor deposited thin-film silicon determined by spectroscopic ellipsometry. *Appl Phys Lett*. 1993;62:3348–3350.

[53] Heavens OS. Optical properties of thin films. *Reports Prog Phys*. 1960;23:1.

[54] Schanda J. *Colorimetry: understanding the CIE system*. Hoboken (NJ): Wiley; 2007.

View publication stats

Supplementary Information
Rendering $Ti_3C_2T_x$ (MXene) Monolayers Visible

A. Miranda,[1] J. Halim,[2] A. Lorke,[1] and M. W. Barsoum[2]

[1] Department of Physics and CENIDE, Universität Duisburg-Essen, Duisburg 47057, Germany
[2] Department of Materials Science and Engineering, Drexel University, Philadelphia, Pennsylvania 19104, USA

The Supplementary Information is comprised of 4 sections:
S1) Procedure for the comparison of experimental data with simulations
S2) Visibility of MXene under illuminant D65
S3) Differentiating between MXene mono and bilayers
S4) Visibility of MXene monolayers on various substrates.

S1) <u>Procedure for the comparison of experimental data with simulations</u>

Here we show the block diagrams used to evaluate the experimental contrasts of the MXene flakes and compare them to the simulated ones.

All images were taken with an optical microscope, OM, (Zeiss Axiotech) equipped with a camera (Canon EOS 500D), with a 100X objective lens (Zeiss Epiplan) with a numerical aperture, NA, of 0.75.

When the optical images were taken they differed in two respects relative to the simulated ones. First the luminosity of the background under the OM is not ideal, viz. $P < 1$ in Eq. 3 of main text. Thus the luminosity had to be extrapolated in order to recalibrate the images [1,2]. As the luminosity is a multiplicative parameter in the XYZ components, to calibrate the images, the XYZ coordinates of an image was divided by P of that image.
Second, the use of a finite numerical aperture, NA, got the objective lens, implies that the light is no perfectly perpendicular to the substrates as in the simulation but with a distribution of incident angles, usually described a Gaussian distribution with a minimum incident angle:

$$\theta_{min} = n \arcsin (NA)$$

where n is the refractive index of air [3]. The different light paths modify the reflectivity of the material for that specific angle, and the total reflectivity must thus be calibrated accordingly [4-7]. However it was shown in Refs. 2 and 3, that the total color difference is not affected significantly by a variation of the NA, and thus herein we neglect this effect.

Apart from these main effects a perfect correspondence between image and simulation is never fully reachable, as several uncontrollable factors play a role. For instance, the calibration of the light source and white balancing might not be ideal, the literature values of the refractive indices of the materials which might differ form those of the investigated materials, and complex digital microscopy hardware and software, which are hard to model and not ideal, to name a few [1].

In Fig. S1(a), the average RGB values for the SiO_2 substrate are extracted from the pictures, and then converted to LAB coordinates. The luminosity and thickness of the SiO_2 is obtained by minimizing the TCD between the experimental LAB values and those calculated for a range of these parameters.

In Fig. S1(b), the RGB values for all the figure (both substrate and MXene) are calibrated according to the illumination extracted in a, and converted to CIELab. The TCD for the thickness calculated in Fig. S1(a) is obtained by averaging the values of the new calibrated figure.

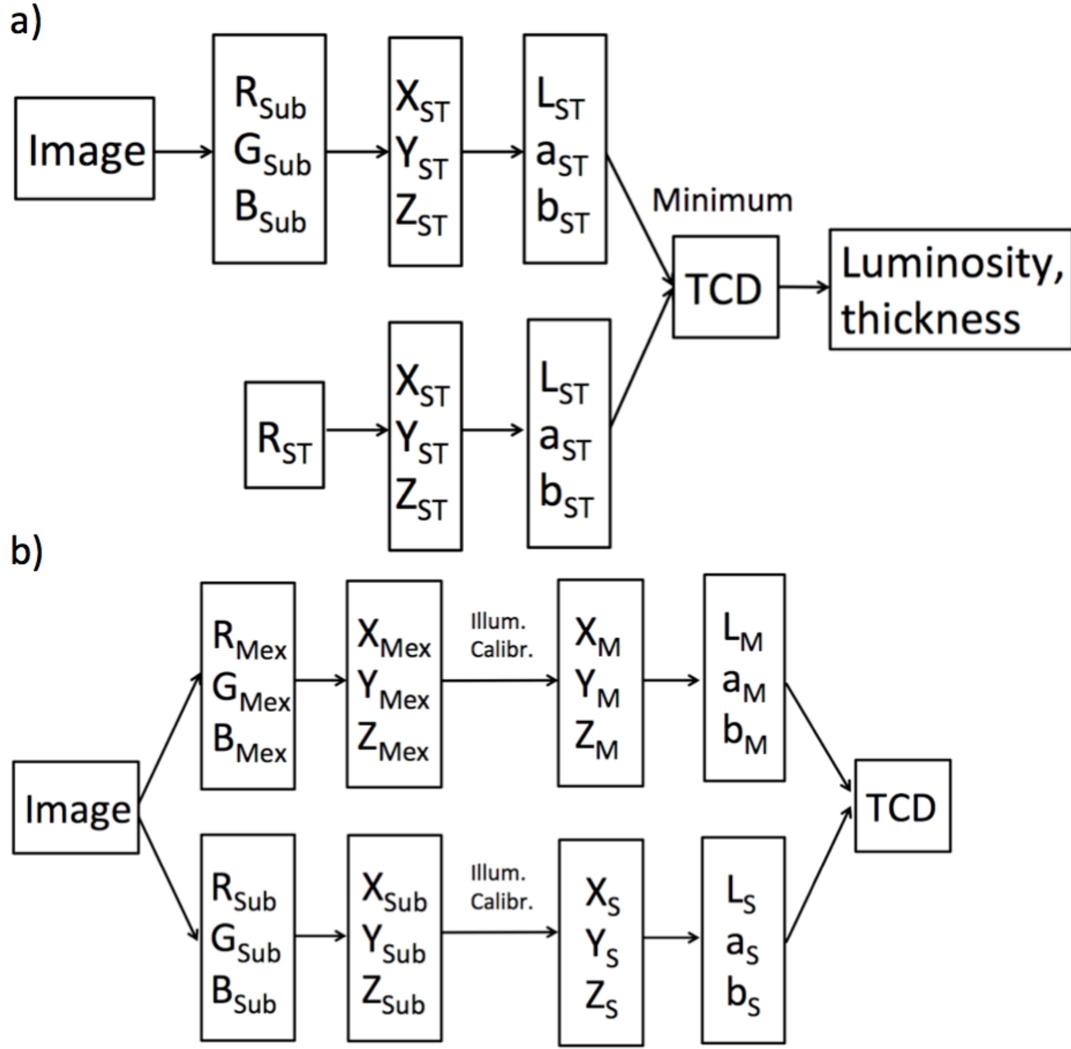

Fig. S1. Schematic of the process for comparison of experimental pictures with simulations as in Fig. 5 in main text.

The algorithm of comparison is divided in two parts: in the first part the luminosity and thickness of the substrate are extracted from the experimental image. In the second part, the image is calibrated in order to have the same luminosity as the simulation (P = 1 in Eq. 3 in main text), and the TCD is extracted.

In Fig. S1(a) we show a schematic of the first part of the algorithm. The RGB coordinates of the substrate of the image are extracted, converted to XYZ coordinates [8], and then to Lab coordinates. These coordinates are compared through the TCD with those obtained by a double loop of the program for the SiO_2/Si substrate, in which both the thickness of the dielectric and the luminosity are treated as parameters.

The couple of parameters that minimize the total color difference is the thickness (0 nm to 400 nm) and luminosity P (1% to 100%) of the experimental image.

As noted in the main text, the thickness for similar substrates was also measured through a profilometer to confirm their values.

Figure S1(b) shows the second part of the algorithm. In this case, the RGB values for MXene and substrate are extracted, transformed into XYZ coordinates, recalibrated by dividing them for the luminosity P, and finally transformed to CIELab coordinates. The TCD of these last coordinates are the effective experimental values that are compared with the simulated ones.

A wide selection of pixels representing the substrate and MXene was chosen for the comparison, and the error bars in Fig. 5 of the main text represent the double standard deviation of the TCD, with the mean value being in the center of the error bar.

S2) Visibility of MXene under illuminant D65

The simulations in the main text were performed using illuminant A, which is defined by the CIE as intended to "represent typical, domestic, tungsten-filament lighting. Its relative spectral power distribution is that of a Planckian radiator at a temperature of approximately 2856 K. CIE standard illuminant A should be used in all applications of colorimetry involving the use of incandescent lighting, unless there are specific reasons for using a different illuminant" [9]. Illuminant A is defined by the spectral density law

$$S_A(\lambda) = 100\left(\frac{560}{\lambda}\right)^5 \frac{exp\frac{1.435\times10^7}{2848\times560}-1}{exp\frac{1.435\times10^7}{2848\times\lambda}-1}$$

where λ is the wavelength in nanometers in standard air. This spectral density function is defined for wavelengths of the visible spectrum (380 – 780 nm) and is normalized to exactly 100 at a wavelength of 560 nm. The tristimulus values for illuminant A are defined as (X, Y, Z) = (109.85, 100.00, 35.58)

Since most present day observations on MXenes are performed on OMs illuminated by a bulb source, we chose illuminant A for the simulations. However, as MXene research evolves, more likely than not, large flakes will be produced will can be visible by the naked eye in natural daylight illumination conditions. This environment is not described correctly by illuminant A and other illuminants should be adopted for the simulations.

The CIE defines: 'CIE standard illuminant D65 as "intended to represent average daylight and has a correlated color temperature of approximately 6500 K. CIE standard illuminant D65 should be used in all colorimetric calculations requiring representative daylight, unless there are specific reasons for using a different illuminant. Variations in the relative spectral power distribution of daylight are known to occur, particularly in the ultraviolet spectral region, as a function of season, time of day, and geographic location. However, CIE standard illuminant D65 should be used pending the availability of additional information on these variations" [9].

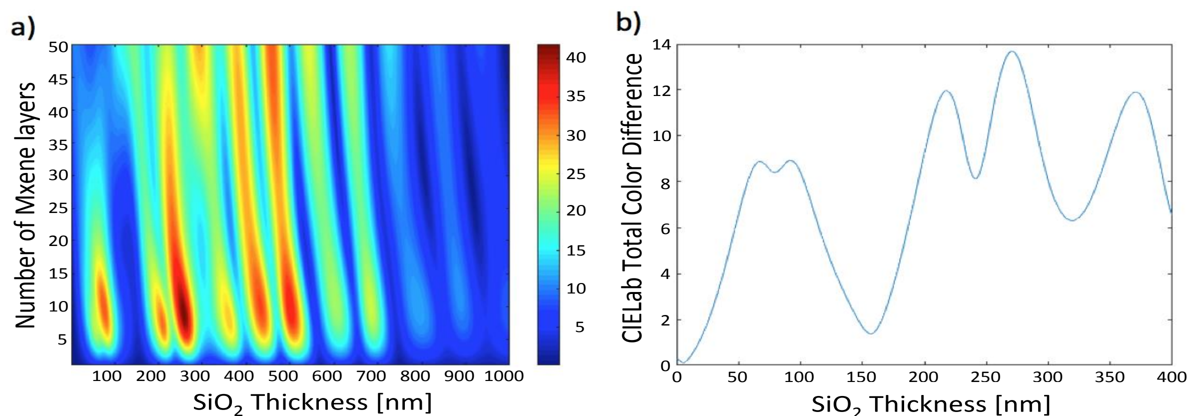

Figure S2. Color plot of CIELab total color difference between SiO_2 and $Ti_3C_2T_x$ monolayers as a function of the number of the latter and the thickness of the former observed under a illuminant D65, delineating the experimental conditions for which the contrast would be greatest. (b) Total color difference of a $Ti_3C_2T_x$ monolayer as a function of the SiO_2 layer thickness. Not surprisingly this plot is quite similar to the one shown in Fig. 5(a).

The values of illuminant D65 are tabulated [10], and it has tristimulus values (X, Y, Z) = (95.04, 100.00, 108.88). Color plot of CIELab total color difference between SiO_2 and $Ti_3C_2T_x$ monolayers as a function of the number of the latter and the thickness of the former observed under a illuminant D65, delineating the experimental conditions for which the contrast would be greatest are shown in Fig. S2(a). Figure S2(b) shows the total color difference of a $Ti_3C_2T_x$ monolayer as a function of the SiO_2 layer thickness. Not surprisingly this plot is similar to the one shown in Fig. 6(a).

S3) Differentiating between MXene mono and bilayers

For a correct identification of a MXene monolayer, it is not only important to identify the MXene flakes on a substrate but be able to rapidly discern whether the flakes are mono- or bilayered [11]. Figures S3(a) and (b), respectively, show the total color difference plots as a function of SiO_2 thickness and λ for bilayer $Ti_3C_2T_x$ MXene and substrate, and for bilayer and monolayer MXene. Regions colored red delineate the experimental conditions for which the contrast would be greatest. Figures S3(c) and (d) plot, the total color difference as a function of the SiO_2 thickness for $Ti_3C_2T_x$ bilayer $Ti_3C_2T_x$ MXene and substrate, and for bilayer and monolayer MXene, respectively. Not surprisingly the differences are quite subtle.

We can take these simulations further. In Figure S4, we simulate the colors of $Ti_3C_2T_x$ single and bilayers on SiO_2 substrates of different thicknesses ranging from 5 nm to 400 nm in steps of 5 nm. In this figure the top centered rectangle simulates the bilayer and the bottom-centered rectangle simulates a monolayer. In all cases contrast in higher between the bilayer and substrate than between monolayer and substrate. The simulations were simulated to have a luminosity of 100% and as seen through a NA = 0. Not surprisingly and in agreement with the results shown in Fig. S3(c) and (d), there are thicknesses for which the $Ti_3C_2T_x$ flakes are almost invisible and other regions where the contrast is quite high.

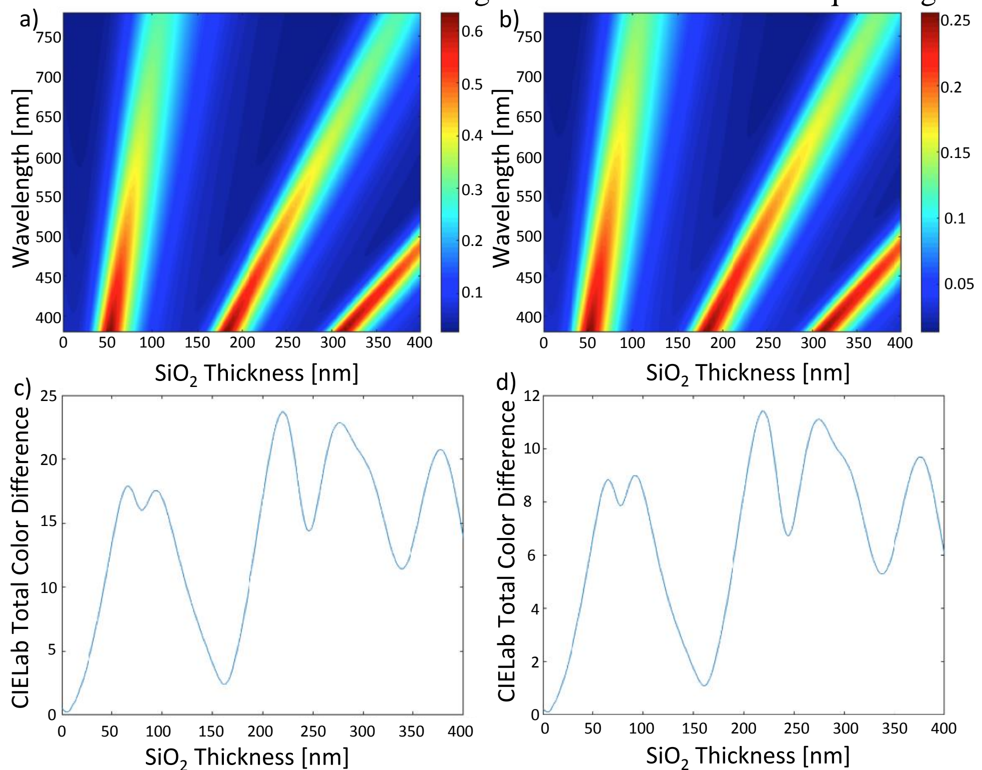

Figure S3. Color plot of the contrast as a function of SiO_2 thickness and λ for (a) bilayer $Ti_3C_2T_x$ MXene and substrate and, (b) bilayer and monolayer $Ti_3C_2T_x$ MXene. Note the strong dependence on both λ and SiO_2 thickness. Dependence of total color difference on SiO_2 layer thickness for a (c) bilayer $Ti_3C_2T_x$ and substrate, and (d) bilayer and monolayer $Ti_3C_2T_x$ MXene.

In addition, we show in Fig. S5(a), and (b) how a $Ti_3C_2T_x$ MXene monolayer would appear on 222 nm, and 280 nm thick SiO_2 layer substrates, that is under the conditions of best visibility. The insets reproduce the experimental results closest to these values (223 nm and 285 nm respectively) for comparison; the agreement between the two is striking.

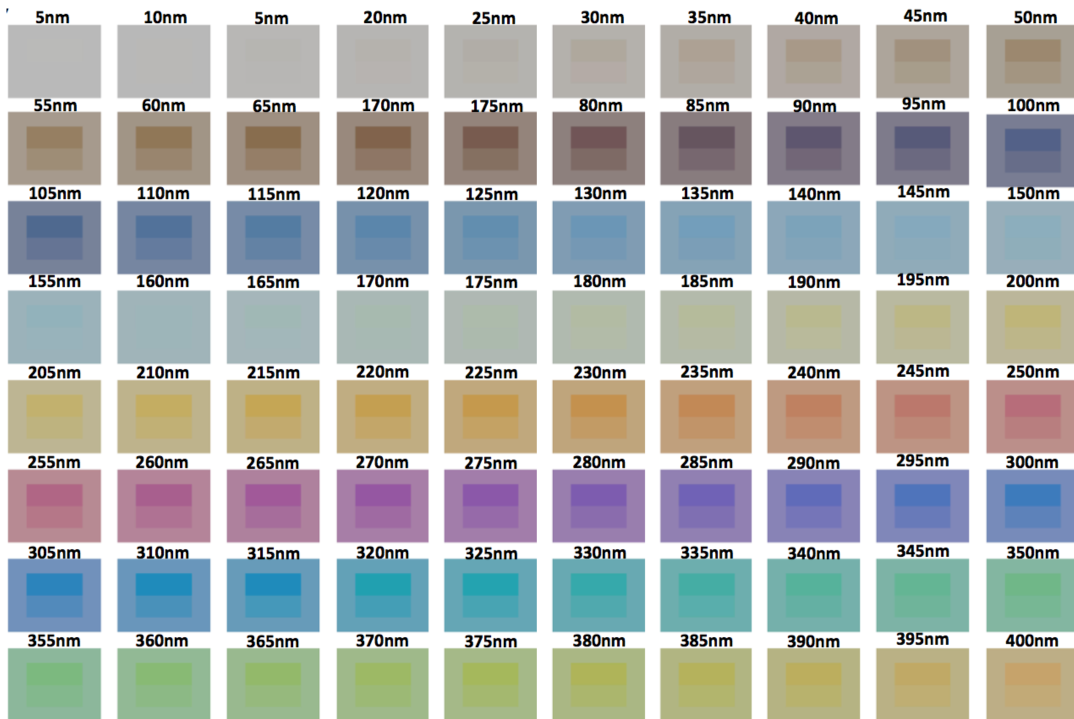

Figure S4. Simulated colors of SiO_2 on Si – with thicknesses ranging from 5 nm to 400 nm - covered by a $Ti_3C_2T_x$ monolayer (bottom centered rectangle) or a bilayer (top centered rectangle). In all cases contrast in higher between the bilayer and substrate than between monolayer and substrate.

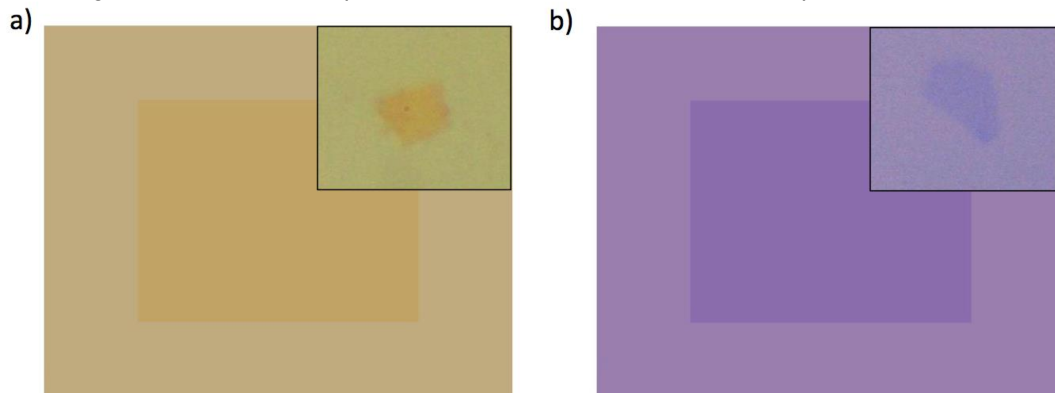

Figure S5. Simulated colors of a rectangular monolayer MXene flake deposited in the center of a SiO_2 substrate with a thickness chosen for optimal visibility: (a) 222 nm and (b) 280 nm. Insets show the corresponding experimental results, viz. 223 nm and 285 nm.

S4) Visibility of monolayer Ti_3C_2 flakes on other substrates

All the calculations so far were performed on SiO_2 on Si substrates. To render this work more useful and applicable to other substrates we also performed simulations of contrast as a function of dielectric thickness where the dielectric was Al_2O_3 on Si (Fig. S6(a)) [12, 13], Si_3N_4 on Si (Fig. S6(b)) [12, 14, 15], HfO_2 on Si (Fig. S6(c))) [12, 16] and Al_2O_3 on Al (Fig. S6(d)) [13, 17], by inserting the relevant refractive indices in the algorithm.

Lastly, Figure S7, shows the effect of the number of $Ti_3C_2T_X$ layers and dielectric thickness values on Al_2O_3 on Si (Fig. S7(a)), Si_3N_4 on Si (Fig. S7(b)), HfO_2 on Si (Fig. S7(c)) and Al_2O_3 on Al (Fig. S7(d)). Interestingly, the results vary quite significantly for each system. Al_2O_3/Al, is the system for which both the contrast and total color difference reach their maximum value among the peaks.

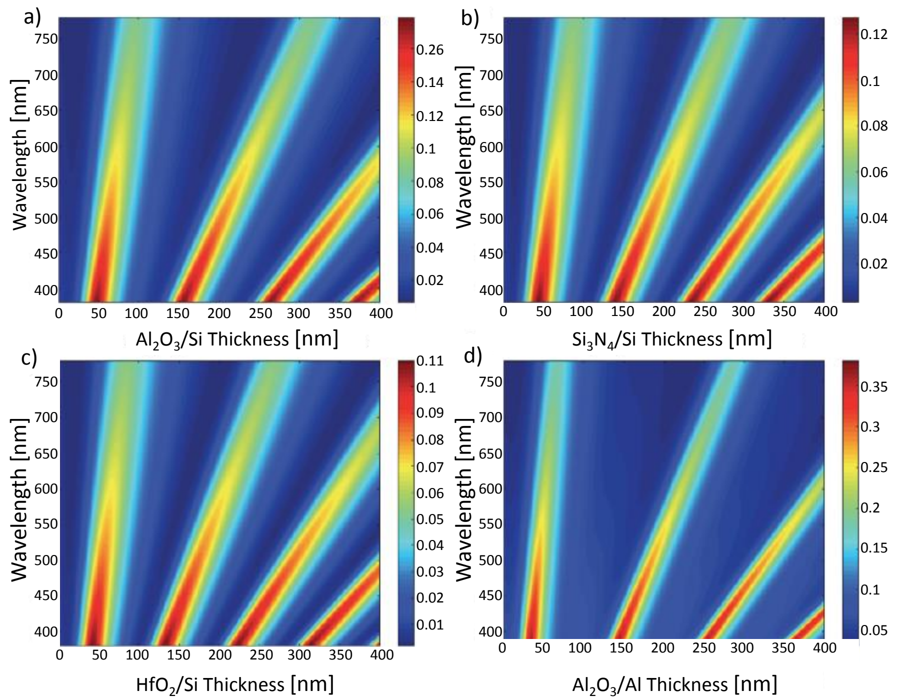

Figure S6. Contrast of $Ti_3C_2T_x$ monolayers as a function of λ and various thicknesses of (a) Al_2O_3/Si, (b) Si_3N_4/Si, (c) HfO_2/Si, and (d) Al_2O_3/Al.

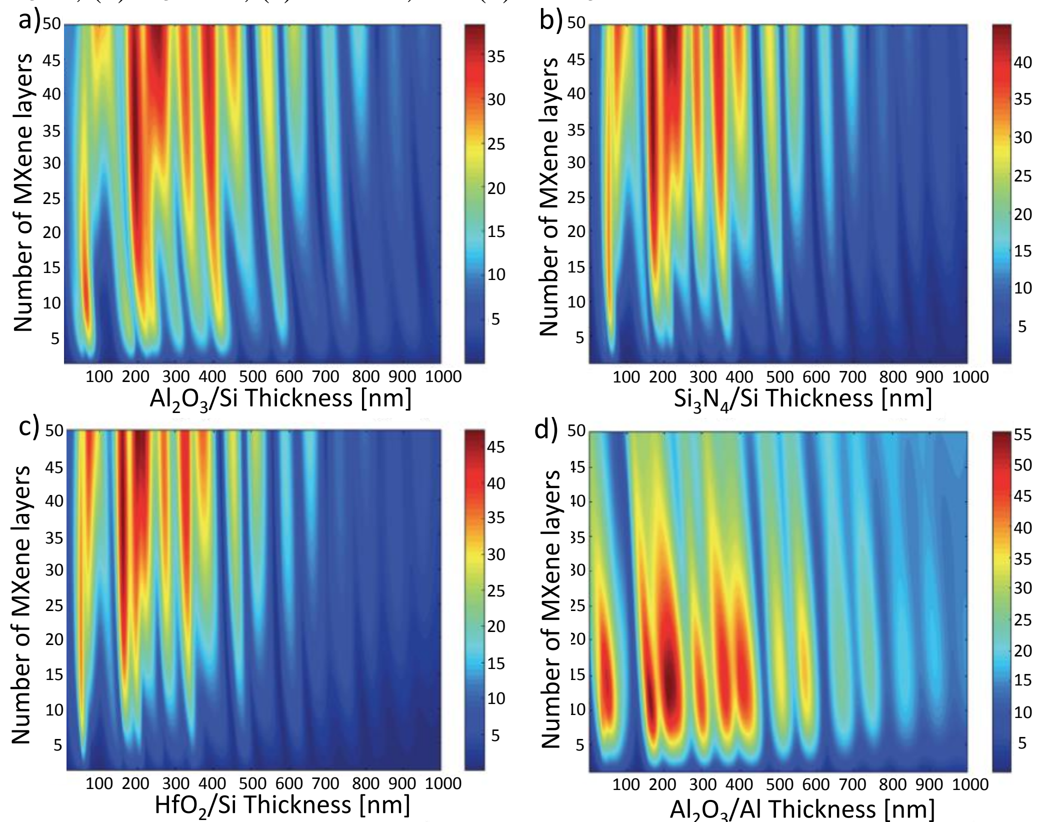

Figure S7. CIELab TCD of 1 to 50 MXene layers as a function of various thicknesses of (a) Al_2O_3/Si, (b) Si_3N_4/Si, (c) HfO_2/Si, and (d) Al_2O_3/Al.

References :

1. Müller MR, Gumprich A, Ecik E, Kallis KT, Winkler F, Kardynal B, et al. Visibility of two-dimensional layered materials on various substrates. J Appl Phys. 2015 Oct 14;118(14):145305.

2. Ouyang W, Liu X-Z, Li Q, Zhang Y, Yang J, Zheng Q. Optical methods for determining thicknesses of few-layer graphene flakes. Nanotechnology. 2013 Dec 20;24(50):505701.

3. Ciddor PE. Refractive index of air: new equations for the visible and near infrared. Appl Opt. 1996 Mar 20;35(9):1566.

4. Gao L, Ren W, Li F, Cheng H-M. Total Color Difference for Rapid and Accurate Identification of Graphene. ACS Nano. 2008 Aug;2(8):1625–33.

5. Jung I, Rhyee J-S, Son JY, Ruoff RS, Rhee K-Y. Colors of graphene and graphene-oxide multilayers on various substrates. Nanotechnology. 2012 Jan 20;23(2):025708.

6. Jung I, Pelton M, Piner R, Dikin DA, Stankovich S, Watcharotone S, et al. Simple Approach for High-Contrast Optical Imaging and Characterization of Graphene-Based Sheets. Nano Lett. 2007 Dec;7(12):3569–75.

7. Roddaro S, Pingue P, Piazza V, Pellegrini V, Beltram F. The Optical Visibility of Graphene: Interference Colors of Ultrathin Graphite on SiO_2. Nano Lett. 2007 Sep;7(9):2707–10.

8. http://www.brucelindbloom.com/.

9. ISO 10526:1999/CIE S005-1998 [Internet]. [cited 2016 Nov 6]. Available from: http://www.cie.co.at/publ/abst/s005.html

10. International Commission on Illumination, Technical Committee TC-1.3 Colorimetry. A method for assessing the quality of daylight simulators for colorimetry. Paris: Bureau central de la CIE; 1981.

11. Nolen CM, Denina G, Teweldebrhan D, Bhanu B, Balandin AA. High-Throughput Large-Area Automated Identification and Quality Control of Graphene and Few-Layer Graphene Films. ACS Nano. 2011 Feb 22;5(2):914–22.

12. Jellison GE. Optical functions of silicon determined by two-channel polarization modulation ellipsometry. Opt Mater. 1992;1(1):41–7.

13. Malitson IH. Refraction and Dispersion of Synthetic Sapphire. J Opt Soc Am. 1962 Dec 1;52(12):1377.

14. Philipp HR. Optical properties of silicon nitride. J Electrochem Soc. 1973;120(2):295–300.

15. Bååk T. Silicon oxynitride; a material for GRIN optics. Appl Opt. 1982;21(6):1069–72.

16. Wood DL, Nassau K, Kometani TY, Nash DL. Optical properties of cubic hafnia stabilized with yttria. Appl Opt. 1990 Feb 1;29(4):604.

17. McPeak KM, Jayanti SV, Kress SJP, Meyer S, Iotti S, Rossinelli A, et al. Plasmonic Films Can Easily Be Better: Rules and Recipes. ACS Photonics. 2015 Mar 18;2(3):326–33.